Wood anomaly transmission enhancement in fishnet-based metamaterials at terahertz frequencies

N. Soltani, Eric Lheurette, D. Lippens

Wood anomaly transmission enhancement in fishnet-based metamaterials at terahertz frequencies

Cite as: J. Appl. Phys. **112**, 124509 (2012); https://doi.org/10.1063/1.4769744
Submitted: 19 July 2012 • Accepted: 13 November 2012 • Published Online: 19 December 2012

N. Soltani, É. Lheurette and D. Lippens

Wood anomaly transmission enhancement in fishnet-based metamaterials at terahertz frequencies

N. Soltani, É. Lheurette, and D. Lippens
IEMN - CNRS UMR 8520, Université de Lille 1, Villeneuve d'Ascq 59652, France

(Received 19 July 2012; accepted 13 November 2012; published online 19 December 2012)

On the basis of a fishnet-like structure, we analyze a metamaterial design involving dimer aperture arrays. It is shown that this approach leads to very strong Fano resonances within the transmission spectrum. The role of the Wood anomaly in the enhancement of the magnetic field is pointed out in order to explain this transmission characteristic. A sensitivity numerical analysis of this resonant feature is carried out. A figure of merit, defined as the ratio between the sensitivity and the width at half maximum of the resonance, as high as 830, is obtained. To our knowledge, this value is greater than the ones reported so far in literature using the inter-particle electromagnetic induced transparency principle. This property is of great interest for environment control applications, especially for sensing of highly diluted media, such as gaseous phase pollutants, as a complement to conventional spectroscopy techniques. © *2012 American Institute of Physics*.
[http://dx.doi.org/10.1063/1.4769744]

I. INTRODUCTION

Metamaterials structures have been widely studied over the last decade. Depending on the design and on the frequency range of interest, metamaterials based devices are able to bring new applications such as invisibility cloaking[1–3] and focusing below the diffraction limit.[4–6] One can also expect performance improvement in the framework of existing application domains, such as filtering at microwaves[7,8] and antennas.[9,10] The world of electromagnetic chemical and gas sensing is dominated by surface plasmon resonance (SPR) sensors operating from visible to infrared wavelengths. These devices take benefit of surface plasmon propagation occurring in metals when the operating frequency becomes significant with respect to their plasma one. Considering the great potential of terahertz spectrum for sensing, the design of high performance electromagnetic sensors targeting this frequency domain is of great interest. Back in 2004, Pendry proposed to use a structured metal in order to decrease the bulk plasma frequency, thus getting access to lower frequency regions of the electromagnetic spectrum.[11] This proposal, based on the concept of metamaterial, is a consequence of the description of a metallic array by an effective permittivity dispersion function. On other hand, the idea of structuring the metallic layer of a sensor has been widely used in SPR design, thus leading to the acronym of LSPR standing for Localized Surface Plasmon Resonance. One can think that when the period of the metallic array is much lower than the working wavelength, these two approaches, arising from two different research fields, are converging.

Over the past few years, the concept of electromagnetic induced transparency (EIT) has been applied to the design of metamaterial sensing devices.[12–14] This phenomenon is often described as the consequence of the coupling between bright (radiating) and dark (non radiating) states in order to induce a sharp feature in the transmission spectrum, thus leading to an enhancement of the sensing sensitivity.[15] One way to reach this working condition is to introduce an asymmetry in a polarization dependant unit-cell.[13,16] However, EIT phenomenon has also been observed from symmetric patterns. In this case, the transparency is induced by the coupling between symmetric and anti-symmetric resonance modes.[17] Most of these published studies use single metallic layer metamaterial structures.

In this paper, we show that very high sensitivities can be obtained from a double layer metamaterial by combining the magnetic activity at the origin of the left-handed band and lattice resonance related to the so-called Wood anomaly. This term was introduced by Wood in 1902 (Ref. 18) when he first observed very sharp variations of diffracted light intensity for a continuous variation on the length of a wave impinging on a metallic grating. The Wood anomaly was interpreted in 1965 by Hessel and Oliner[19] as the superimposition of two distinct phenomena occurring at the Rayleigh wavelength. The first one is the redistribution of diffraction orders over higher spatial harmonics. The second one is the lattice resonance involving the contribution of the complex wave along the plane of the grating.

In Sec. II, we detail the design steps of the metamaterial device. In Secs. III and IV, the transmission spectrum is analyzed with the help of finite element simulator, using a global description by means of transmission spectrum and a local analysis of electromagnetic field maps. On the basis of these characteristics, an enhancement of the magnetic field related to the Wood anomaly is pointed out. Finally, in Sec. V, the sensing capabilities of the metamaterial are evaluated through the sensing sensitivity and figure of merit.

II. METAMATERIAL DESIGN

The sensing device has been inspired from our previous designs of double negative metamaterials for terahertz frequencies.[20,21] The original structure involved stacked metallic thin films perforated by elliptical apertures and separated by uniform benzocyclobutene (BCB) interlayers. Initially, the

period along the propagation direction was 26 μm, which is equivalent to $\lambda/25$ at the operating frequency of 0.5 THz, thus insuring a metamaterial condition for a wave vector normal to the metallic planes. We have shown that the use of elliptical holes with a typical elliptical aspect ratio (*EAR*) greater than 1.6:1 enhances the transmission level for an incident electric field polarized along the small axis of the ellipse. This property is a consequence of impedance matching between the metamaterial and the impinging plane wave.[22] The negative refraction of this fishnet-like metamaterial has been experimentally demonstrated both indirectly, by means of Fresnel relations inversion retrieval from reflection and transmission measurements[23] and directly, from angular measurements at the wedged interface of a prism prototype.[21]

The structure we introduce in this article has been downscaled in order to reach operating frequencies around 1 THz. Then, the stacking has been limited to a couple of metallic layers, which is the minimal condition to create a magnetic activity through the combination of conductive currents on the metallic plates and displacement current in the dielectric interlayer. The third modification, by anticipating towards sensing applications, is the structuring of the BCB interlayer in order to enable the absorption of a chemical element under test in the apertures where the electromagnetic energy is strongly localized. It is important to note that this structuring of the BCB apertures is easily achievable by reactive ion etching process. Besides, the size reduction, as a consequence of downscaling, remains compatible with standard photolithography patterning.

III. TRANSMISSION SPECTRUM ANALYSIS

The metamaterial structures have been simulated with the finite element solver *HFSS* developed by *Ansoft*. This structure, whose unit cell is depicted in Figure 1, is illuminated under normal incidence with the electric field direction along the small axis of the ellipse as indicated in the inset. For these simulations, the unit cell is bounded by periodic conditions along the O_X and O_Y directions, which insure the repetition of the elementary pattern as an infinite slab. In order to describe the propagation of the electromagnetic wave along the O_Z direction, wave ports are located at a typical distance of 150 μm above and below the unit cell. Gold has been modeled considering a finite conductivity $\sigma = 4.1 \times 10^7$ S/m whereas the relative permittivity of the BCB interlayer is equal to 2.6. In the following, we reported the reflection and transmission frequency spectra for two distinct values of the short axis diameter a_Y. The other dimensions are the ones reported in the caption of Figure 1. The basic transmission figure shows an anti-resonance feature followed by a transmission band. This evolution reveals the opening of a left-handed band as attested by the dispersion diagrams, obtained by a Fresnel relations inversion method, which is detailed in Ref. 19. The dispersion diagram representation describes the evolution of the normalized complex propagation constant versus frequency: $\gamma \cdot {}^{a}/_{\pi} = (\alpha + j\beta) \cdot {}^{a}/_{\pi}$ where a, α, and β are the propagation distance, attenuation constant, and phase constant, respectively. It is important to note here that the attenuation constant is positive over the whole frequency band. This is consistent with the fact that the metamaterial, which is a passive device, does not behave as an amplifying media. Positive values of β along with near-zero values of α reveal a right-handed transmission band. On the contrary, negative values of β along with near-zero values of α are the signature of a left-handed transmission band.

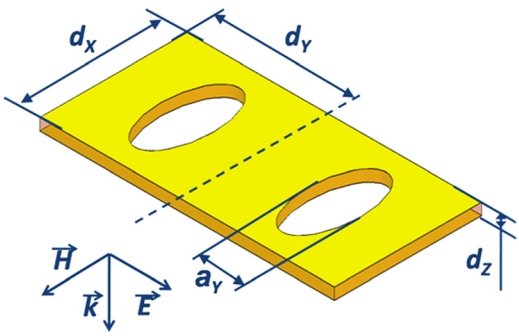

FIG. 1. Unit cell of the metamaterial sensing structure: $d_X = d_Y = 170\ \mu$m, $EAR = 2$, metal thickness $= 0.4\ \mu$m, BCB interlayer $= 13\ \mu$m. Inset: Schematic of the polarization configuration.

In the first situation, illustrated by Figures 2 and 3, the transmission level in the left-handed band ($f \sim 0.95$ THz) is very close to unity. This result is obtained for a short axis diameter a_Y of 76 μm, which permits to satisfy an impedance matching condition as explained in Ref. 21. The dispersion diagram shows left- and right-handed bands separated by a vanishing band-gap, giving rise to a continuous evolution including negative, zero and positive values of the refractive index. Considering these two characteristics, this first structure can be considered as optimized for free-space transmission applications, such as frequency and spatial angular filtering.

In the second situation (Figure 4: $a_Y = 58\ \mu$m), this left-handed transmission maximum decreases slightly below -5 dB since the impedance matching is degraded as a consequence of a reduction of the elliptical aperture area. Moreover, a wide band gap is occurring, restricting the right-handed dispersion branch (Figure 5). This design is not interesting for the applications mentioned before. However, one can take benefit of the sharp feature of the transmission

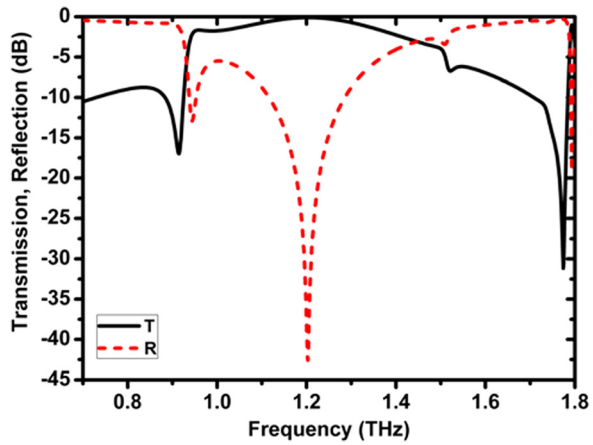

FIG. 2. Reflection and transmission spectra of a symmetrical fishnet array designed for an operating frequency of 1 THz: $d_X = d_Y = 170\ \mu$m, $a_Y = 76\ \mu$m, $EAR = 2$, and $d_Z = 13\ \mu$m.

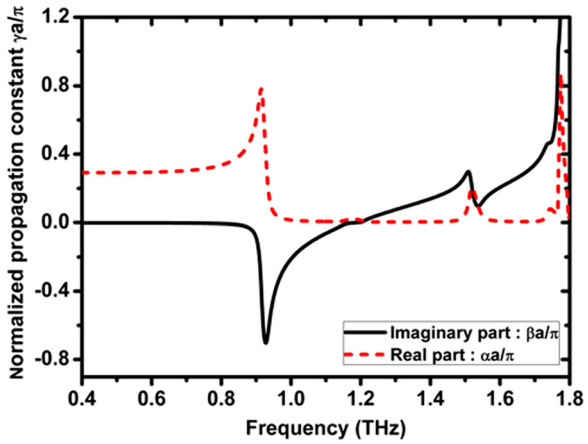

FIG. 3. Dispersion diagram of a symmetrical fishnet array designed for an operating frequency of 1 THz: $d_X = d_Y = 170\ \mu$m, $a_Y = 76\ \mu$m, $EAR = 2$, and $d_Z = 13\ \mu$m.

characteristic, including the anti-resonance followed by the left-handed transmission peak, for sensing applications.

Each of the transmission spectra depicted in Figures 2 and 4 includes a very sharp dip slightly beyond 1.8 THz. The position of this dip, independent of the hole diameter, is related to the so-called Wood anomaly, which corresponds to a redistribution of the energy through a higher diffraction order.[18,19,24,25]

This first numerical study illustrates the great potential of our fishnet metamaterial, which can lead to various transmission and dispersion spectra with the control of the short-axis diameter a_Y as a single parameter. In order to sharpen the transmission characteristic, with an expected benefit on detection sensitivity for sensing applications, we need to introduce an additional geometrical parameter. Following this general idea, a new metamaterial structure is introduced and discussed in Sec. IV.

IV. ANALYSIS OF THE HALF-ELLIPSE (HE) METAMATERIAL STRUCTURE

When progressively modifying the geometry of the apertures from full ellipse (FE) to half-ellipse patterns, very

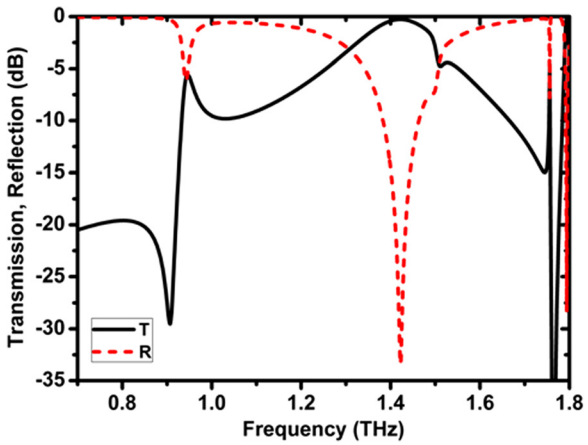

FIG. 4. Reflection and transmission spectra of a symmetrical fishnet array designed for an operating frequency of 1 THz: $d_X = d_Y = 170\ \mu$m, $a_Y = 58\ \mu$m, $EAR = 2$, and $d_Z = 13\ \mu$m.

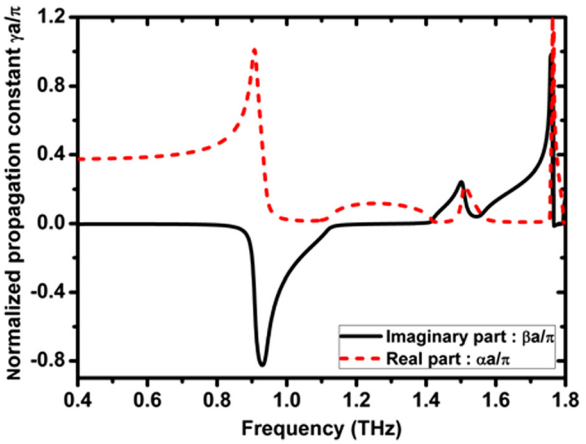

FIG. 5. Dispersion diagram of a symmetrical fishnet array designed for an operating frequency of 1 THz: $d_X = d_Y = 170\ \mu$m, $a_Y = 58\ \mu$m, $EAR = 2$, and $d_Z = 13\ \mu$m.

sharp transmission peaks occur, as depicted in Figure 6. In this graph, the horizontal axis describes the closing process of the elliptical hole. For instance, 0 μm corresponds to the whole elliptical apertures (black lower transmission curve in Figure 7) while 29 μm corresponds to the half ellipse (brown higher transmission curve on Figure 7).

In the following, we focus on the case of the half ellipse, which can be considered as an optimal geometry for sensing, taking into account the sharpness of the ground transmission peak occurring before the left-handed band. It should be noted that this geometrical modification leads to asymmetrical apertures. In this scheme, another unit cell including two half-ellipse apertures has to be defined (Figure 8). The evolution towards this dimer scheme is illustrated on the right side of Figure 7. This gradual modification of the geometry has two main consequences. First, the additional transmission

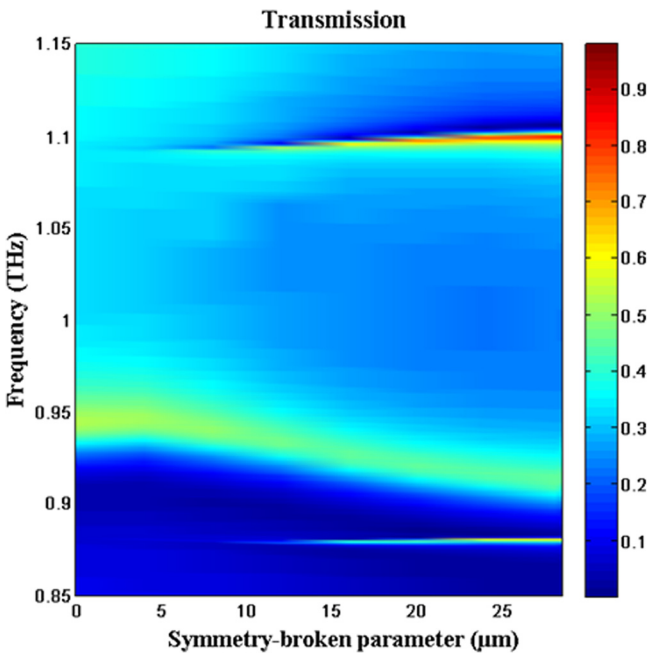

FIG. 6. Parametric analysis showing the occurrence of two resonant features when elliptical apertures are progressively closed.

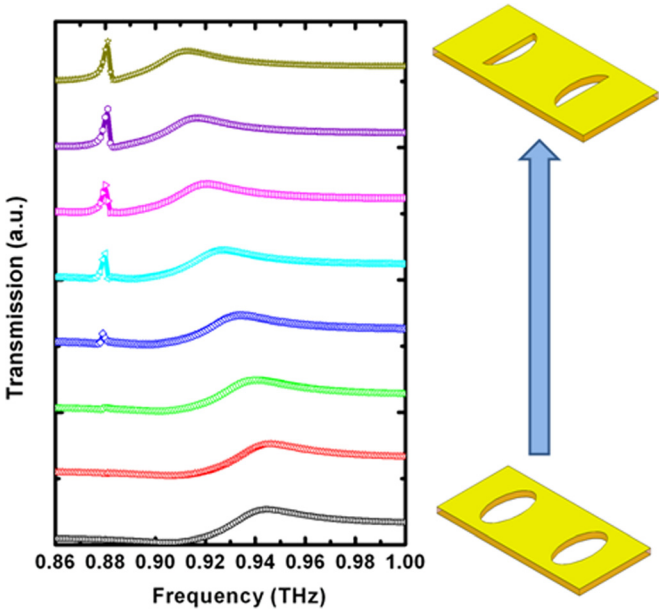

FIG. 7. Transmission curves reported on a shifted scale versus frequency when the elliptical apertures are progressively closed.

peak is increasing when moving from the FE to the HE arrays. The frequency of this peak remains constant and equal to 0.881 THz. Second, the left-handed transmission band is globally shifted to lower frequencies. This red-shift is not related to a reducing of the aperture area because this would have the opposite consequence of blue-shifting the left transmission band. Indeed, the left-handed branch position depends on the plasma electric frequency, which is strongly dependent on the cut-off frequency of the aperture. Such a tendency can be observed for slight closing of the apertures as it is illustrated by the comparison of the black and red curves of Figure 7. When the apertures are further closed, it seems reasonable to consider the red-shift as a signature of the evolution to the dimer unit-cell. This hypothesis is confirmed by the frequency position of the occurring transmission peak, which is very close to the first order Wood frequency associated to the doubled periodicity d_Y (340 μm). This frequency is defined by the ratio between the velocity of light c and the periodicity d_Y. The relationship between the peak position and the Wood frequency is further commented in the following.

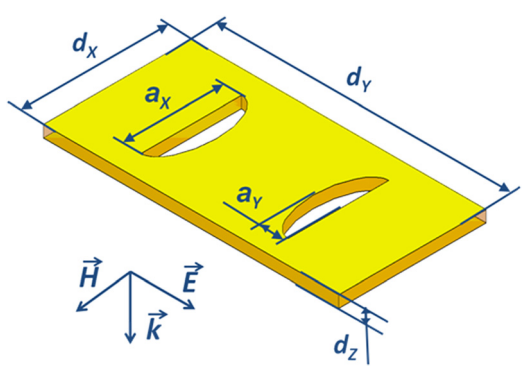

FIG. 8. Unit cell of the HE metamaterial structure: $d_X = 170\,\mu$m, $d_Y = 340\,\mu$m, $a_Y = 29\,\mu$m, $a_X/a_Y = 4$, metal thickness $= 0.4\,\mu$m, BCB interlayer $= 13\,\mu$m. Inset: Schematic of the polarization configuration.

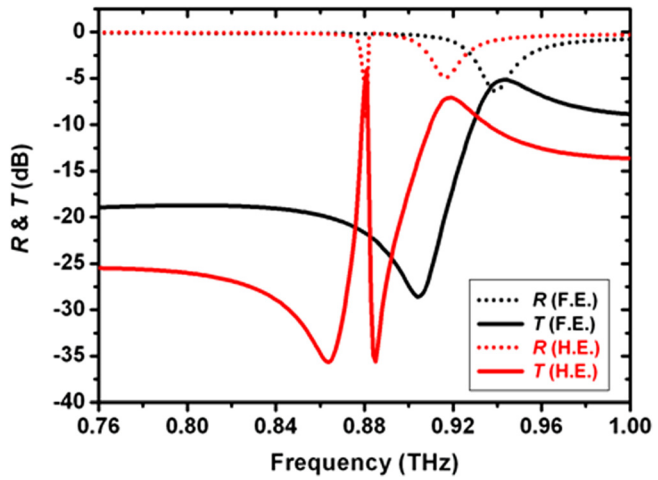

FIG. 9. Transmission and reflection spectra corresponding to the FE and HE arrays.

In Figure 9, we compare the transmission spectra of the FE and HE arrays. Using a restricted frequency scale, we can see that the 0.881 THz frequency peak is located just before the ground left-handed transmission band. In this case, one can take benefit of a very low transmission background due to the well-known anti-resonance phenomenon, which corresponds to the π phase jump to the edge of the first Brillouin zone. Indeed, the left handed-transmission band is always preceded by a dip related to the magnetic resonance of the coupled metallic plates reported in Refs. 20 and 23. This vicinity has the consequence of increasing the transmission contrast within this frequency range. This highly contrasted transmission means high quality coefficient, which is a welcome property for sensing applications.

When considering the doubled period d_Y, as a consequence of the dimer introduction, the ratio between the velocity of light and d_Y is equal to 0.8823 THz, which is an intermediate value between the peak (0.881 THz) and the dip (0.885 THz) frequencies observed in Figure 9. This Fano-like resonance[26] involving a peak and a dip in close vicinity is the consequence of a lattice resonance giving rise to

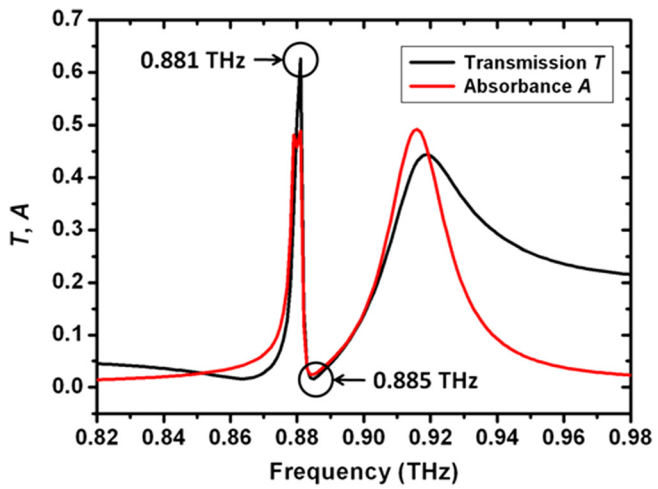

FIG. 10. Magnitude of the transmission and absorbance as a function of frequency for the half-ellipse array.

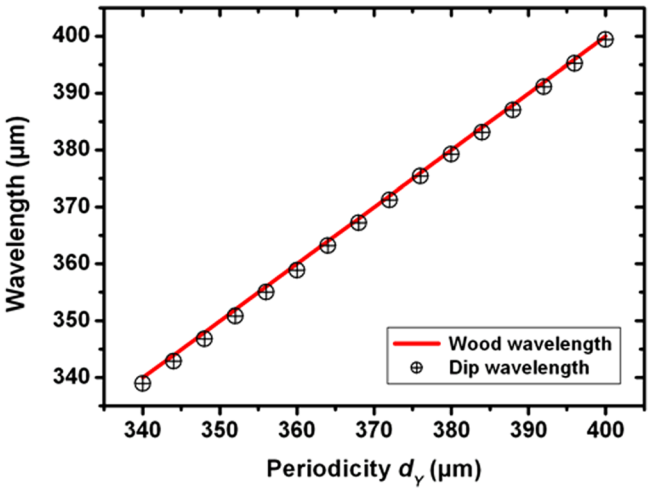

FIG. 11. Wavelength of the dip as a function of the periodicity d_Y: numerical simulations (symbols) and analytical calculation (red line).

a wave propagating in the plane of the structured media. In order to make the distinction between this surface wave and the Wood anomaly, one can use the criterion of absorbance (Figure 10). In fact, as mentioned before, the Wood anomaly which corresponds to a redistribution of impinging energy is a lossless phenomenon. In this case, the absorbance should be very close to zero. This is what we observe at the frequency of 0.885 THz corresponding to the dip in the transmission. On the contrary, the propagation of a plasmon-like wave is dissipative. This is the reason of the absorbance peak observed at 0.881 THz.

In order to strengthen the interpretation of a dimer array, which doubles the initial periodicity, we plotted the evolution of the wavelength related to the dip as a function of the periodicity d_Y (Figure 11). One can attest the perfect linearity of this evolution, which can be superimposed on the Wood anomaly wavelength determined by the c/d_Y ratio. It should be noted that the doubling of the period also introduces higher order resonances that are beyond the scope of this study.

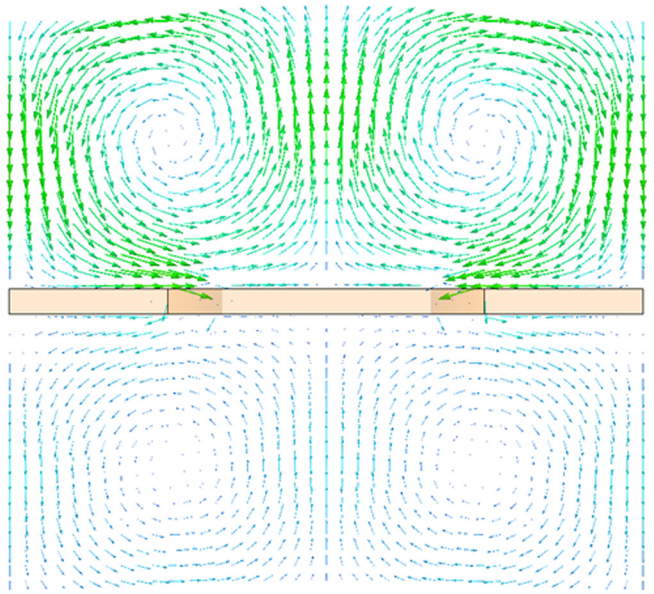

FIG. 12. Poynting vector flow in the *YZ* cut plane at 0.881 THz.

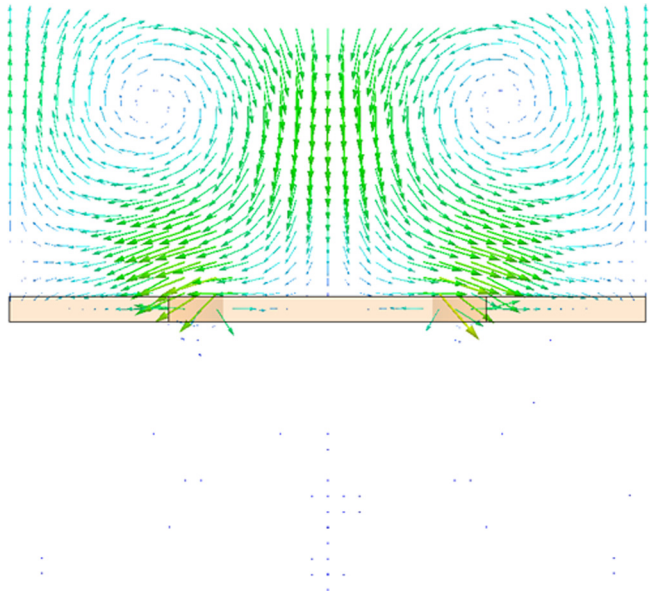

FIG. 13. Poynting vector flow in the *YZ* cut plane at 0.885 THz.

The relationship between the Wood anomaly and the highly contrasted transmission spectrum can be understood by means of the field maps given from Figures 12 to 17. These plots include the Poynting vector (Figures 12 and 13), the electric and magnetic field magnitudes (Figures 14 and 15), and the surface currents on the outer faces of the BCB interlayer (Figures 16 and 17). Each of these quantities is plotted at the peak (0.881 THz) and dip (0.885 THz) transmission frequencies.

First, the Poynting vector gives a global description of the electromagnetic energy flow across the structure. The injection port is located on the top of the structure. Vortices like patterns are clearly evidenced both at 0.881 and 0.885 THz.

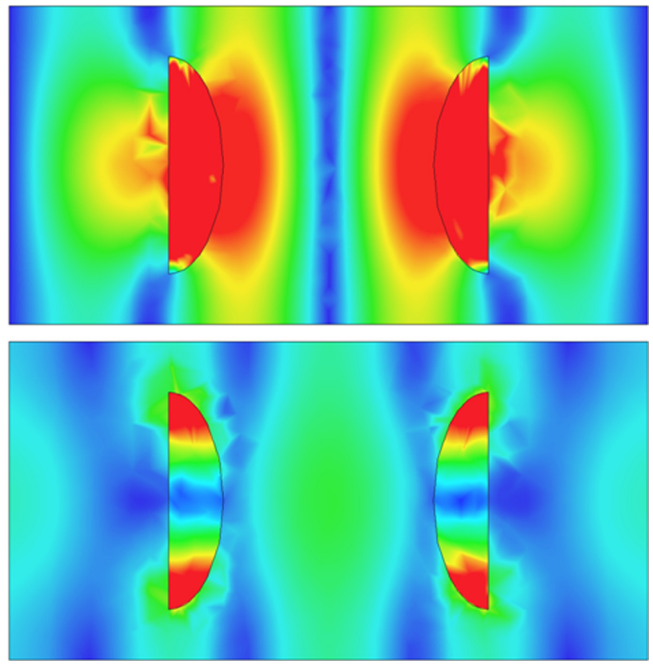

FIG. 14. Magnitudes of the electric (top view) and magnetic fields probed in the BCB mid plane for $f = 0.881$ THz.

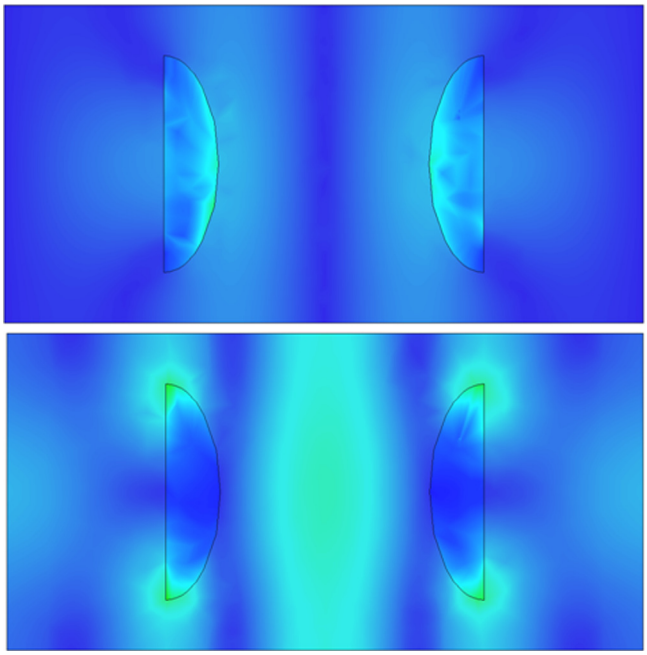

FIG. 15. Magnitudes of the electric (top view) and magnetic fields probed in the BCB mid plane for $f = 0.885$ THz.

These patterns are typical of the Wood anomaly lattice resonance.[27] At 0.881 THz, the electromagnetic energy couples to the lower half plane by means of the apertures whereas at 0.885 THz, the energy is reflected in the upper half plane. This is a direct illustration of the Fano resonance observed on the transmission curve.

The observation of electric, magnetic, and current maps in the structure brings a deeper understanding on this specific transmission response. Although some color plots are saturated due to the high transmission contrast, we preferred using the same scale for both the peak (0.881 THz) and dip (0.885 THz) in order to facilitate the comparison between these two situations. Therefore, for both frequencies, electric field magnitudes are plotted with a linear scale ranging from 0 (blue) up to 400 000 V/m (red) whereas magnetic field magnitudes are plotted with a linear scale ranging from 0 (blue) up to 3000 A/m (red).

First, it appears clearly that the coupled apertures in the back to back configuration behave like a dimer. Indeed, the electric and magnetic field maps are typical of a magnetic resonance situation with a concentration of the electric field on the edges of the dimer and a concentration of the magnetic field between the apertures, which play the role of subparticles in the dimer scheme. At 0.885 THz, the location of the magnetic field concentration between the holes is coherent with the observation of Parsons and co-workers.[28] However, the structure we study differs by the specificity of a higher concentration between the two-sub particles of the dimer. The contours of these field maps are globally similar at the peak and dip frequencies. However, at 0.881 THz, which correspond to the transmission peak (Figure 14), one can note an important increase of the magnetic field amplitude inside the apertures.

The magnetic field resonance observation is confirmed by the surface currents maps of Figures 16 and 17 plotted on the top and bottom faces of the BCB interlayer. These maps show an anti-parallel configuration of the currents, which corresponds to an anti-symmetric resonance mode at the origin of the well known current loop in the coupled nanorod type metamaterial particles.[29] At 0.881 THz, the current plot on the bottom surface shows a maximum value on the edges of the apertures, which is consistent with the previous

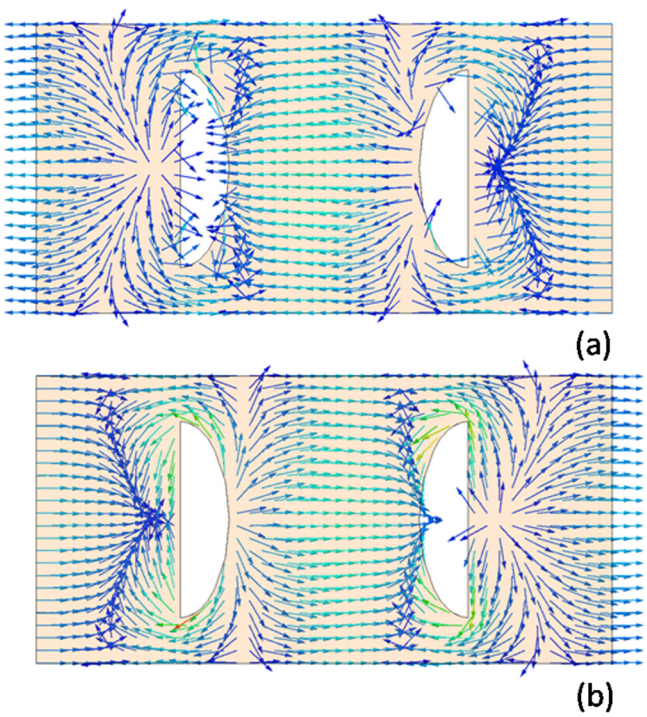

FIG. 16. Surface current plots on the top face (a) and bottom face (b) of the BCB interlayer at 0.881 THz.

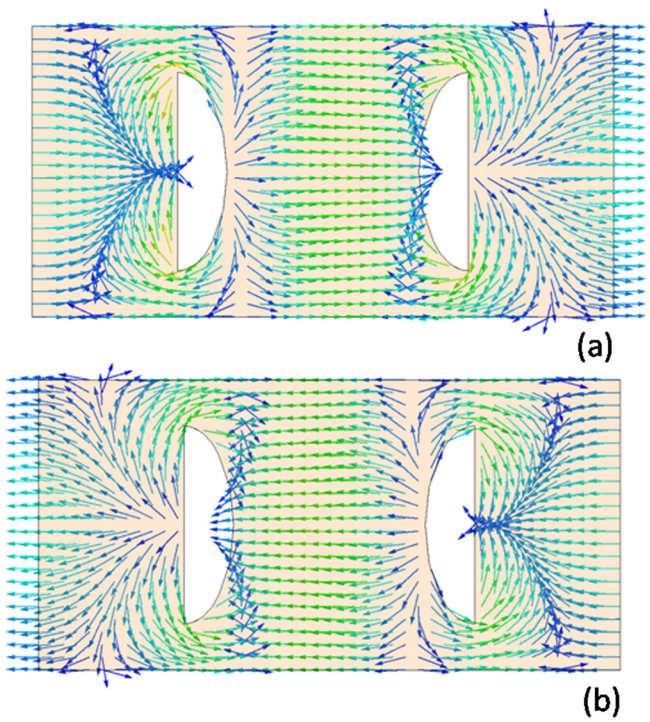

FIG. 17. Surface current plots on the top face (a) and bottom face (b) of the BCB interlayer at 0.885 THz.

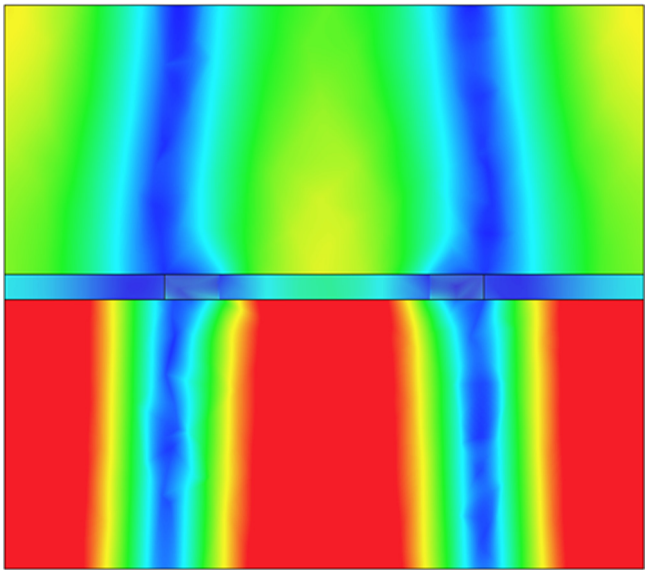

FIG. 18. Magnitude of the magnetic field in the *YZ* cut plane at 0.881 THz.

comments on the magnetic field concentration. From these local observations, one can conclude that the transmission peak is related to an enhancement of the magnetic field, which results from the combination between the magnetic resonance of metallic surfaces facing each other and the lattice resonance related to the Wood anomaly.

This enhancement is directly evidenced by plotting the field map magnitude in the *YZ* cut plane (Figures 18 and 19). For both these plots, the linear magnitude scale is ranging from 0 (blue) up to 4000 A/m (red). Whereas the magnitude of the magnetic field is decreasing in the lower half-plane at 0.885 THz as expected, a huge increasing is observed at the peak frequency (0.881 THz). Such a phenomenon has been reported recently by Tang and co-authors[30] on arrays of coupled nanorods at optics. However, the structure proposed here is quite different as it is based on a fishnet configuration,

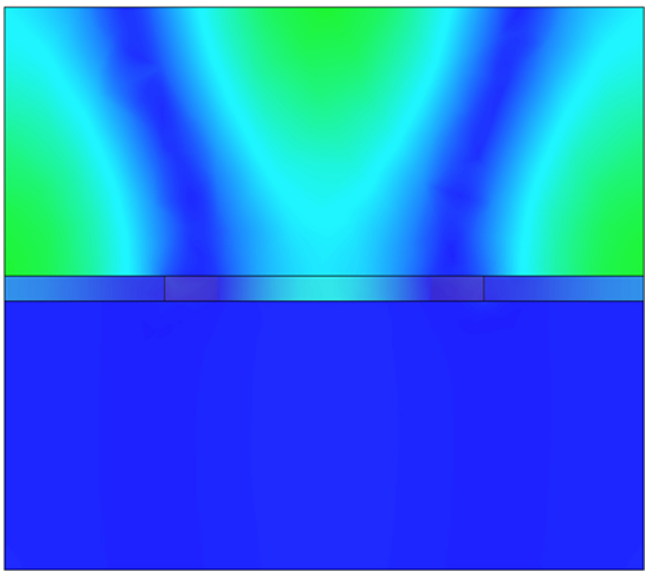

FIG. 19. Magnitude of the magnetic field in the *YZ* cut plane at 0.885 THz.

which behaves like a double negative media. Moreover, the introduction of the doubled periodicity d_Y ($d_Y = 340\,\mu$m), by means of the dimer configuration, brings the Wood frequency slightly below the ground transmission band instead of the value expected around 1.8 THz for the initial metamaterial ($d_Y = 170\,\mu$m).

These characteristics are interesting for various research domains. As general prospects, one can take benefit of the strong dispersion related to the Fano resonance characteristic for slow light applications.[12,31,32] In addition, the enhancement of the magnetic field occurring in our structure can be a first step to the exploitation of nonlinearities.[33–35] As a more immediate application, one can think about the great potential of the very sharp transmission feature in order to improve the sensitivity of sensing devices. Following this direction, further elements are given in Sec. V.

V. SENSING PROPERTIES

The terahertz spectrum is a powerful tool for gas spectroscopy as several gases have strong signatures within this frequency range. The gas spectroscopy techniques are mainly based on direct absorption measurements, targeting signatures of specific molecules within the terahertz spectrum. On other hand, the SPR techniques take benefit of the plasmon resonance shift when the refractive index of the atmosphere in the vicinity of the metallic surface is modified. This sensing principle is the same for the metamaterial proposed here with a potential extension of the frequency range through a specific scale engineering of the metallic layers. Figure 20 shows a frequency shift of typically 10 GHz for a fluctuation of the surrounding refractive index as small as 0.01. In Figure 21, we have plotted the sensitivity $S = \Delta\lambda/\Delta n$ versus the refractive index of the media surrounding the device. $\Delta\lambda$ is the wavelength shift, in nanometer, obtained for the refractive index variation Δn. The very high values of S, typically several 100 000 are mainly due to the fact that the wavelength unit is the nanometer, whereas the working wavelength is about 500 μm. In order to alleviate this scaling factor, we also plotted the figure of merit defined as follows:

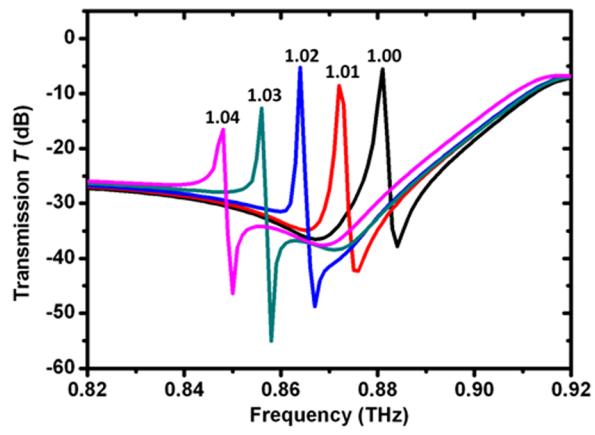

FIG. 20. Transmission coefficient versus frequency for different index values of the surrounding media.

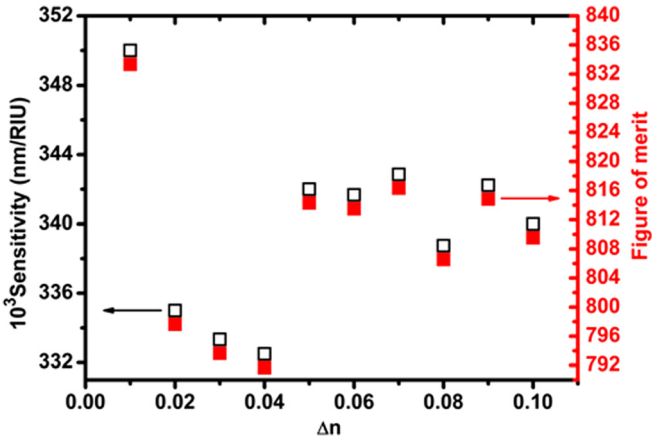

FIG. 21. Sensitivity and figure of merit evolutions versus the differential refractive index.

$$FOM = \frac{S(nm/RIU)}{FWHM(nm)},$$

where *FWHM* is the full width at half maximum of the resonant feature. The values we obtain, as high as 830, overcome the ones published so far using EIT inspired inter-particle coupling. One has to take into account the fact that this numerical result would undoubtedly be minored in the context of experience. Nevertheless, this appears like a promising approach for the design of high sensitivity sensors.

VI. CONCLUSION

We proposed a design of sensing metamaterial based on the fishnet-structure. We showed that by using double metallic layer structure including dimer type unit-cells, one can take benefit of a very high quality Fano resonance explained as follows: The introduction of the doubled periodicity by means of the dimer configuration brings the Wood lattice resonance in close vicinity of the ground transmission band. This gives rise to a very sharp transmission feature due to an enhancement of the magnetic resonance. This design, which leads to figures of merit of several hundred at terahertz frequency range, is promising for sensing applications in this spectral domain, which is considered as essential for gas detection and biological investigations.

ACKNOWLEDGMENTS

The authors would like to thank B. Djafari Rouhani, P. Tassin, and J.-L. Coutaz for fruitful discussions.

[1]D. Schurig, J. J. Mock, B. J. Justice, S. A. Cummer, J. B. Pendry, A. F. Starr, and D. R. Smith, Science **314**, 977 (2006).
[2]D. P. Gaillot, C. Croënne, and D. Lippens, Opt. Express **16**, 3986 (2008).
[3]T. Ergin, N. Stenger, P. Brenner, J. B. Pendry, and M. Wegener, Science **328**, 337 (2010).
[4]M. C. K. Wiltshire, J. B. Pendry, and J. V. Hajnal, J. Phys.: Condens. Matter **18**, L315–L321 (2006).
[5]N. Fang, H. Lee, C. Sun, and X. Zhang, Science **308**, 534 (2005).
[6]M. J. Freire, R. Marqués, and L. Jelinek, Applied Physics Letters **93**, 231108 (2008).
[7]J. Garcia-Garcia, J. Bonache, I. Gil, F. Martin, M. C. Velazquez-Ahumada, and J. Martel, IEEE Trans. Microwave Theory Tech. **54**, 2628 (2006).
[8]A. L. Borja, J. Carbonell, V. E. Boria, and D. Lippens, Appl. Phys. Lett. **93**, 203505 (2008).
[9]A. Ourir, S. N. Burokur, and A. de Lustrac, Electron. Lett. **43**, 493 (2007).
[10]P. H. Tichit, S. N. Burokur, and A. de Lustrac, J. Appl. Phys. **105**, 104912 (2009).
[11]J. B. Pendry, L. Martin-Moreno, and F. J. Garcia-Vidal, Science **305**, 847 (2004).
[12]N. Papasimakis, V. A. Fedotov, N. I. Zheludev, and S. L. Prosvirnin, Phys. Rev. Lett. **101**, 253903 (2008).
[13]N. Liu, L. Langguth, T. Weiss, J. Kastel, M. Fleischhauer, T. Pfau, and H. Giessen, Nature Mater. **8**, 758 (2009).
[14]S. Zhang, D. A. Genov, Y. Wang, M. Liu, and X. Zhang, Phys. Rev. Lett. **101**, 047401 (2008).
[15]P. Tassin, L. Zhang, T. Koschny, E. N. Economou, and C. M. Soukoulis, Phys. Rev. Lett. **102**, 053901 (2009).
[16]B. Lahiri, A. Z. Khokhar, R. M. De La Rue, S. G. McMeekin, and N. P. Johnson, Opt. Express **17**, 1107 (2009).
[17]N. Papasimakis, Y. H. Fu, V. A. Fedotov, S. L. Prosvirnin, D. P. Tsai, and N. I. Zheludev, Appl. Phys. Lett. **94**, 211902 (2009).
[18]R. W. Wood, Proc. Phys. Soc., London, Sect. A **18**, 269 (1902).
[19]A. Hessel and A. A. Oliner, Appl. Opt. **4**, 1275 (1965).
[20]C. Croenne, F. Garet, E. Lheurette, J.-L. Coutaz, and D. Lippens, Appl. Phys. Lett. **94**, 133112 (2009).
[21]S. Wang, F. Garet, K. Blary, E. Lheurette, J.-L. Coutaz, and D. Lippens, Appl. Phys. Lett. **97**, 181902 (2010).
[22]J. Carbonell, C. Croenne, F. Garet, E. Lheurette, J.-L. Coutaz, and D. Lippens, J. Appl. Phys. **108**, 014907 (2010).
[23]S. Wang, F. Garet, K. Blary, C. Croenne, E. Lheurette, J.-L. Coutaz, and D. Lippens, J. Appl. Phys. **107**, 074510 (2010).
[24]M. Sarrazin, J.-P. Vigneron, and J.-M. Vigoureux, Phys. Rev. B **67**, 085415 (2003).
[25]F. J. Garcia de Abajo, Rev. Mod. Phys. **79**, 1267 (2007).
[26]A. E. Miroshnichenko, S. Flach, and Y. S. Kivshar, Rev. Mod. Phys. **82**, 2257–2298 (2010).
[27]J. M. Steele, C. E. Moran, A. Lee, C. M. Aguirre, and N. J. Halas, Phys. Rev. B **68**, 205103 (2003).
[28]J. Parsons, E. Hendry, J. R. Sambles, and W. L. Barnes, Phys. Rev. B **80**, 245117 (2009).
[29]V. M. Shalaev, W. Cai, U. K. Chettiar, H.-K. Yuan, A. K. Sarychev, V. P. Drachev, and A. V. Kildishev, Opt. Lett. **30**, 3356 (2005).
[30]C. J. Tang, P. Zhan, Z. S. Cao, J. Pan, Z. Chen, and Z. L. Wang, Phys. Rev. B **83**, 041402 (2011).
[31]C. Wu, A. B. Khanikaev, and G. Shvets, Phys. Rev. Lett. **106**, 107403 (2011).
[32]B. Qiang, L. Cong, C. Jing, C. Chen, K. Ming, and W. Hui-Tian, J. Appl. Phys. **107**, 093104 (2010).
[33]Z. Wang, Y. Luo, T. Jiang, Z. Wang, J. Huangfu, and L. Ran, Phys. Rev. Lett. **106**, 047402 (2011).
[34]I. V. Shadrivov, A. B. Kozyrev, D. W. van der Weide, and Y. S. Kivshar, Appl. Phys. Lett. **93**, 161903 (2008).
[35]E. Poutrina, D. Huang, and D. R. Smith, New J. Phys. **12**, 093010 (2010).